

A REDSHIFT $z = 6.56$ GALAXY BEHIND THE CLUSTER ABELL 370¹

E. M. HU,^{2,3} L. L. COWIE,^{2,3} R. J. MCMAHON,^{2,4} P. CAPAK,³ F. IWAMURO,⁵ J.-P. KNEIB,⁶
T. MAIHARA,⁷ K. MOTOHARA⁸

Submitted to the Astrophysical Journal Letters

ABSTRACT

We report the discovery of a redshift $z = 6.56$ galaxy lying behind the cluster Abell 370. The object HCM 6A was found in a narrowband imaging survey using a 118 Å bandpass filter centered at 9152 Å in the LRIS camera on the 10 m Keck II Telescope. Candidate Ly α emitters were identified by the equivalent width of the emission and the absence of lower wavelength flux in ultradeep broadband images. HCM 6A is the first galaxy to be confirmed at redshift $z > 6$, and has $W_\lambda(\text{observed})=190$ Å, flux = 2.7×10^{-17} erg cm⁻² s⁻¹. Spectra obtained with LRIS confirm the emission line and the continuum break across the line, and show an asymmetric line profile with steep fall-off on the blue side. Deep Subaru near-infrared CISCO images in J , H and K' which extend the sampled continuum to longer wavelengths give a consistent estimate of the continuum flux density in these line-free regions of $2.6 \pm 0.7 \times 10^{-30}$ erg cm⁻² s⁻¹ Hz⁻¹. The line width and strength, asymmetric profile, and very deep spectral break are only consistent with the interpretation of the line as a redshifted Ly α feature. From the detailed lensing model of this cluster, we estimate a lensing amplification of 4.5 for this galaxy, which is located slightly over an arcminute from the center of the cluster, for an unlensed flux of 6.5×10^{-18} erg cm⁻² s⁻¹. The presence of such a galaxy suggests that the reionizing epoch is beyond $z = 6.6$.

Subject headings: cosmology: observations — early universe — galaxies: distances and redshifts — galaxies: evolution — galaxies: formation

1. INTRODUCTION

The study of the early universe through high-redshift galaxies has seen substantial progress in recent times, with a number of galaxies discovered at redshifts $z > 5$ (Dey et al. 1998; Hu, Cowie, & McMahon 1998; Weymann et al. 1998; Hu, McMahon, & Cowie 1999; Stern & Spinrad 1999; Ellis et al. 2001). Active galaxies associated with radio galaxies (van Breugel et al. 1999) have been seen to similar redshifts and quasars have now been detected out to $z = 6.28$ from the Sloan survey (Fan et al. 2000; Anderson et al. 2001; Fan et al. 2001).

The present letter describes a continuation of our narrowband filter survey (Cowie & Hu 1998; Hu et al. 1998, 1999), which probes Ly α emission from $z = 3.4 \rightarrow 5.7$, to a redshift $z \sim 6.5$. At $z = 3$ the brightest Ly α emitters have line fluxes near 10^{-16} erg cm⁻² s⁻¹ and a single, roughly 30 arcmin² field of the LRIS camera on the Keck 10 m telescope yields a handful of objects to a flux limit of 10^{-17} erg cm⁻² s⁻¹. At $z \sim 6.5$ the fluxes drop to near the sensitivity limit and only occasional objects are expected to be found (e.g., Thommes 1999). Therefore, to improve our sensitivity limits we have targeted foreground massive lensing clusters which can provide substantial amplification over a fraction of the LRIS field. We have also observed the well studied blank fields used in the

shorter wavelength narrowband searches. Even with the increased sensitivity provided by the lensing detections are extremely rare and our observations have so far yielded only one compelling detection lying behind the cluster A370. We describe this object in the present letter.

Discriminating Ly α emitters from lower z emission-line objects can be difficult at lower redshifts (Stern & Spinrad 1999), but as we move to higher redshifts the continuum break signature becomes so extreme that there is little likelihood of a misidentification provided we have sufficiently deep continuum images. Songaila and Cowie (2002) have used spectra of the Sloan quasars to measure the average transmission of the Ly α forest region as a function of redshift over the $z = 4 \rightarrow 6$ range. Their results translate to a magnitude break across the Ly α emission line of

$$\Delta m = 3.8 + 20.3 \log_{10} \left(\frac{1+z}{7} \right)$$

Extrapolated to $z = 6.5$ this corresponds to a 4.5 magnitude break. If the epoch of reionization is at $z \sim 6.1$ as suggested by Becker et al. (2001), the continuum blueward of Ly α would be essentially black. However, as we shall consider further in the discussion section, in this case the radiation damping wings of the foreground neutral hydrogen extend through the Ly α emission and make it unlikely we would see Ly α emitters at all, so the presence of the

¹ Based in part on data collected at the Subaru Telescope, which is operated by the National Astronomical Society of Japan

² Visiting Astronomer, W. M. Keck Observatory, which is jointly operated by the California Institute of Technology, the University of California, and the National Aeronautics and Space Administration

³ Institute for Astronomy, University of Hawaii, 2680 Woodlawn Drive, Honolulu, Hawaii 96822

⁴ Institute of Astronomy, Madingley Road, Cambridge CB3 0HA, U.K.

⁵ Department of Physics, Kyoto University, Kitashirakawa, Kyoto 606-8502, Japan

⁶ Observatoire Midi-Pyrénées, 14 Avenue E. Belin, 31400 Toulouse, France

⁷ Department of Astronomy, Kyoto University, Kitashirakawa, Kyoto 606-8502, Japan

⁸ Institute of Astronomy, University of Tokyo, 2-21-1 Osawa, Mitaka, Tokyo 181-0015, Japan

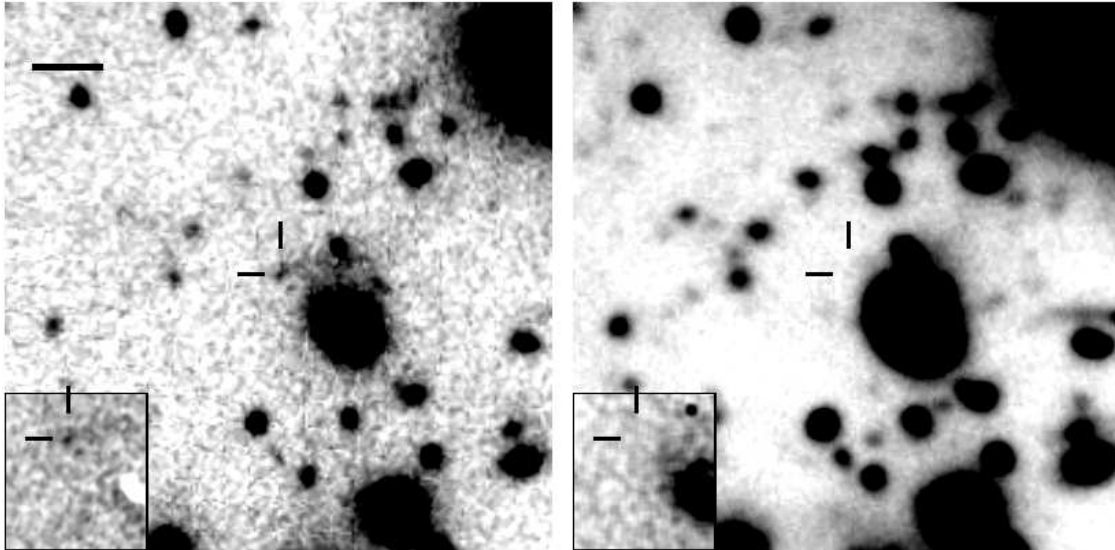


FIG. 1.— Narrowband 9152/118 Å image (left panel) and R -band image (right panel) of the emission-line object HCM 6A, which is marked with the vertical and horizontal lines. An image in the narrowband filter with a normalized local continuum (Z band) subtracted (inset in left panel) shows that the object, which appears as two fragments, is a strong emission-line object. (We have slightly oversubtracted the Z band to completely remove the neighboring galaxy, whose core appears white.) The galaxy is not seen in the much deeper R -band image (> 8 hours on the Keck 10 m Telescope) or in a 5600 s F675W image taken with the WFPC2 camera on HST, shown in the insert in the right hand panel. The neighboring bright galaxy to the SW is a cluster member with a redshift of 0.375 (“BO #39” in Mellier et al. 1988), so that the emission is not associated with this object – in particular $H\alpha$ lies shortward of the filter bandpass. The images are centered on coordinates (J2000) RA: $2^{\text{h}} 39^{\text{m}} 54^{\text{s}}.73$ Dec: $-1^{\circ} 33' 32''.3$ and are $37''$ on a side. The bar in the upper left corner of the narrowband image shows a $5''$ scale.

A370 emitter argues for a higher reionization redshift.

In Section 2 we summarize the narrowband observations and the continuum observations at longer and shorter wavelengths together with the spectroscopic followup. The properties of HCM 6A leave little doubt about its identification as a high- z $\text{Ly}\alpha$ emitter. Finally, in the discussion we consider the implications for early star formation and for the evolution of the intergalactic gas.

2. OBSERVATIONS

2.1. Narrow Band Survey

The present images were obtained using a 118 Å filter centered on 9152 Å in the LRIS camera (Oke et al. 1995) on the Keck 10 m telescopes. This wavelength lies in a very dark region of the night sky between the OH(8-4) and OH(7-3) bands, and corresponds to $\text{Ly}\alpha$ at a redshift of ~ 6.5 . In total, six fields have been imaged with this filter, and are summarized in Table 1. In each case the exposures were made as a sequence of spatially dithered background-limited exposures and median skies were used to flat field the images. The images were calibrated with spectrophotometric standards. The deepest exposures, totaling about 6 hours per field, were taken on the HDF and on fields centered on the clusters A370 and A851. Over most of the area in these fields the 5 sigma limiting flux sensitivity is approximately 1.6×10^{-17} erg cm^{-2} s^{-1} but, for the massive clusters, there is a small area in the central regions where the lensing amplification provides a significant gain in sensitivity.

For each field a very deep Z band ($\lambda_{\text{eff}} \sim 9170$ Å; Hu et al. 1999) was used to measure the continuum and an extremely deep R -band image was used as a shorter wavelength reference to measure the continuum break. We

searched each field for objects with observed equivalent widths in excess of 100 Å which were not visible in the R image. Only one such object has been found in the six fields. Finding images for HCM 6A, which lies behind the massive lensing cluster A370 in a region of significant amplification, are shown in Figure 1, which compares narrowband and deep R continuum images and gives coordinates. Insets show the continuum-subtracted image and the corresponding WFPC2 F675W image from HST. (See Bézecourt et al. (1999) for a description of the wider field of the HST image). The following subsections describe the observations made on this object to confirm that it is a high redshift $\text{Ly}\alpha$ emitter rather than a lower redshift emission-line object.

2.2. Broad Band Optical Imaging

Deep multicolor images of A370 were obtained using LRIS on the Keck 10 m telescopes on UT 1999 August 11, 1999 September 9–10, 2000 August 25, and 2000 December 29 and 2002 January 11–12. The data were taken as a sequence of dithered exposures, with net integration times of 2400 s in V , 27900 s in R , 4050 s in I and 9820 s in Z . A deep B (3780 s) image was obtained with ESI on Keck II on UT 2000 September 29–30. The images were processed using median sky flats generated from the exposures. Conditions were photometric during these observations. The data were calibrated using the photometric and spectrophotometric standard, HZ4 (Turnshek et al. 1990; Oke 1990), and faint Landolt standard stars in the SA 95-42 field (Landolt 1992).

2.3. Near-infrared Imaging

TABLE 1
SUMMARY OF LRIS $\text{Ly}\alpha$ NB9152 SURVEY IMAGING

Field	RA(2000)	Dec(2000)	Exposures	t_{exp} (s)
A370 ^a	02:39:53.1	-01:34:35	14 \times 1500 s	21000
A851 ^a	09:43:02.6	+46:58:58	19 \times 900 s + 7 \times 650 s	21650
HDF	12:36:52.0	+62:12:30	12 \times 1800 s	21600
SSA17	17:06:31.1	+43:55:40	6 \times 1200 s	7200
A2390 ^a	21:53:34.6	+17:40:10	11 \times 1500 s	16500
SSA22	22:17:31.9	+00:15:01	9 \times 1500 s	13500

^a Cluster redshifts are $z = 0.37$ for A370, 0.41 for A851, and 0.231 for A2390.

We used the new Cooled Infrared Spectrograph and Camera for OHS (CISCO, Motohara et al. 1998) on the Subaru 8.3 m Telescope on UT 2000 June 18-19, July 15-16, September 10-12, and November 7 to obtain extremely deep J , H , and K' images of A370. The detector used was a 1024×1024 HgCdTe HAWAII array with a pixel scale of $0.111''$. This provides a field-of-view of $\sim 2' \times 2'$. To minimize the image degradation, a number of sub-exposures were taken at each position in an eight-point pentagon pattern ($5''$ step size). Weather conditions were photometric, and the seeing was typically $0.3'' - 0.5''$ during the first three observing runs, which was also the resolution of nearly all the final reduced images. Conditions were clear, but with variable seeing during the November observing run, with characteristic image FWHM of $\sim 0.8''$ for the A370 H final image. The data were processed using median sky flats generated from the dithered images. The data were calibrated from observations of the UKIRT faint standards (Casali & Hawarden 1992) FS27, FS29, FS6, and FS10. The total exposure times were 13280 s (J), 7680 s (H), and 15360 s (K').

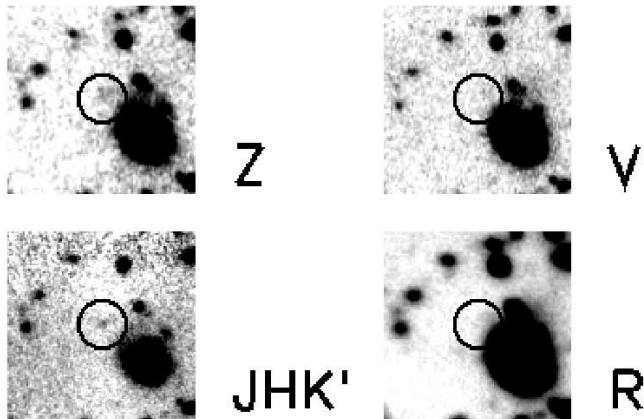


FIG. 2.— Broadband images of the redshift $z = 6.56$ galaxy HCM 6A in colors above the Lyman break (left-hand column) and below the Lyman break (right column). The lower left image marked JHK' is a weighted sum of the J , H , and K' images. The thumbnail images are $19''$ on a side, centered on the position of the emission, and the circles are $1.2''$ in radius.

2.4. Colors and SEDs

HCM 6A is clearly detected at all wavelengths longer than the Z band as is shown in Figure 2, where we present

thumbnail images centered on the object, which is circled (left column). However, it is not seen at any shorter wavelengths (right column).

The spectral energy distribution of HCM 6A is shown in Figure 3, where the error bars are 1 sigma. At wavelengths above the Z band the mean flux density averaged over the J , H , and K' bands is $2.6 \pm 0.7 \times 10^{-30}$ erg cm⁻² s⁻¹ Hz⁻¹ while at shorter wavelengths averaged over the V and R bands the flux density is $0.1 \pm 2.9 \times 10^{-31}$ erg cm⁻² s⁻¹ Hz⁻¹. At the 2 sigma level the continuum break exceeds 1.7 magnitudes.

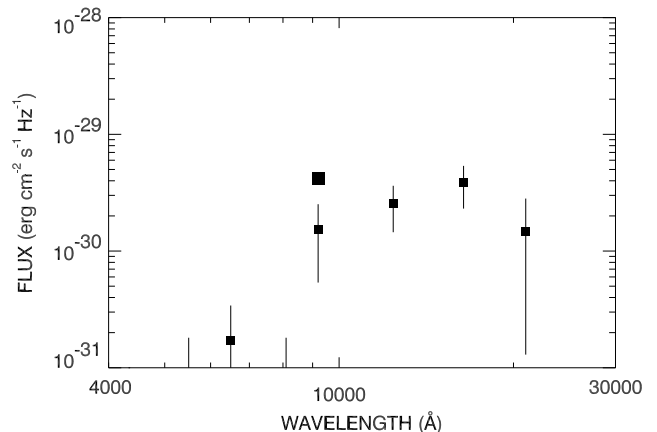


FIG. 3.— The spectral energy distribution of HCM 6A from 4000 Å to 22000 Å. The broad band fluxes (B, V, R, I, Z, J, H, K') are shown with small boxes while the narrowband at 9152\AA is shown with the larger box. The fluxes have been measured in $1''$ diameter apertures centered on the object and the error bars are 1 sigma errors based on similar aperture measurements on clear portions of the field. Note the strong continuum break across the narrowband filter at 9152\AA .

2.5. LRIS Spectroscopy

Spectra of the object were obtained with the LRIS spectrograph during a runs in UT 16–18 September 1999, 23–24 January 2001, and 21 October 2001. The observations were made in multislit mode using $1.4''$ wide slits with a variety of gratings. The emission line is clearly seen in all the spectra, and the stacked spectra show the line profile to be asymmetric, with steeper blue fall-off as would be expected from the effects of the forest absorption. The redward continuum is most clearly seen in the spectra obtained with the 400 l/mm grating, which in combination with the slit width gives a resolution of roughly 11.8\AA , and we show the combined spectra obtained in this mode in Figure 4. The strong emission

line is at a wavelength of 9187 Å, which corresponds to a redshift of $z = 6.56$ for Lyman alpha. The continuum break is consistent with that obtained from the imaging data but is more poorly determined because of the uncertainties in the sky subtraction in the spectra.

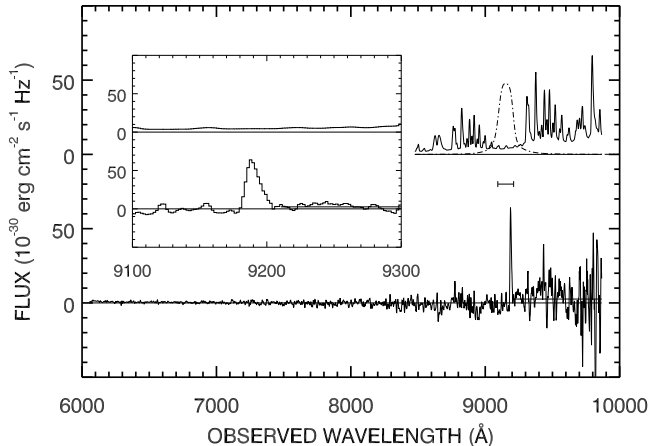


FIG. 4.— The spectrum of HCM 6A from a 4-hr exposure made with the LRIS spectrograph using the 400 line/mm grating. The emission line is at 9187Å. The solid line near the axis shows the median continuum flux above the line, and gives a break strength consistent with the broadband measurements. The solid line above the emission shows the 50% width of the narrowband filter, whose profile is shown overlaid on the fluxed nightsky spectrum, plotted at 1% strength above the object spectrum. Enlarged plots of the object’s emission feature and 1% of the nightsky background spectra taken with the 400 line/mm grating are shown in the inset, where the asymmetry of the line profile can be clearly seen.

3. RESULTS AND DISCUSSION

The absence of detections outside the cluster lensing regions places a 1 sigma upper limit of 27 deg^{-2} for the number of sources in the filter bandpass ($\Delta z = 0.1$) at the 5σ flux limit of $1.6 \times 10^{-17} \text{ erg cm}^{-2} \text{ s}^{-1}$ (the HDF limit) and 13 deg^{-2} at $2.7 \times 10^{-17} \text{ erg cm}^{-2} \text{ s}^{-1}$ (the worst limit in the six fields), which is broadly consistent with that expected from models (e.g., Thommes 1999) or extrapolation from lower redshifts.

We have used the Lenstool model of A370 described in Kneib et al. (1993) to measure an amplification of 4.5 at the position of HCM 6A, giving a demagnified flux of $6 \times 10^{-18} \text{ erg cm}^{-2} \text{ s}^{-1}$. Lenstool also allows us to measure the corresponding source plane areas which would give such amplifications. For the combined A370, A851, and A2390 areas the observed source plane area is 0.46 arcmin^2 , with most of this area lying behind the most massive (A370) cluster. The surface density of objects above a flux limit of $4 \times 10^{-18} \text{ erg cm}^{-2} \text{ s}^{-1}$ is then between 1300 and 26000 deg^{-1} , where the range is $\pm 1 \sigma$, which is also broadly consistent with the model expectations.

Equivalent width determination for very high- z objects is complicated by the strong forest absorption on the blue side of the emission feature, and across the Z band. For the 1 arcsec diameter aperture measurements shown in Fig-

ure 3 the equivalent width determined from the line flux and the average long-wavelength continuum flux above the emission feature is 190 Å. If instead the average Z -band continuum is used as the reference value, the computed equivalent width increases to 325 Å.

The brighter region of the object is clearly extended along an axis of about 110° in PA with a maximum length of around $4''$. The elongation is consistent with the substantial distortion expected at this position if the galaxy lies at very high redshift, providing an additional weak confirmation of the redshift identification. The intrinsic size of the main region at the source plane is then around $1''$. The second fragment lies around $1''$ away from the brighter portion. At $z = 6.56$ with the currently favored Lambda cosmology ($\Lambda = 0.66$ and $\Omega = 0.33$) and $H_0 = 65 \text{ km s}^{-1} \text{ Mpc}^{-1}$ these angular sizes correspond to physical sizes of approximately 40 kpc.

After removing the lensing amplification the continuum flux corresponds to a rest frame ultraviolet luminosity of $2 \times 10^{29} \text{ erg s}^{-1} \text{ Hz}^{-1}$, which may be used to estimate the star formation rate. For a Salpeter IMF extending to $0.1 M_\odot$, this is about $40 M_\odot \text{ yr}^{-1}$. The rest frame demagnified Ly α luminosity is $2 \times 10^{42} \text{ erg s}^{-1}$ which, assuming case B recombination and using Kennicutt’s (1983) translation of H α luminosity to star formation rate, would correspond to a rate of $2 M_\odot \text{ yr}^{-1}$. The lower value obtained from the Ly α luminosity presumably reflects the combined effects of dust extinction in the galaxy and destruction of the blue side of the emission line by scattering in the intergalactic medium.

Using the more robust UV continuum estimate we find that the universal star formation rate at this redshift from this class of object lies in the range $0.13 \rightarrow 2.7 M_\odot \text{ Mpc}^{-3} \text{ yr}^{-1}$ ($\pm 1 \sigma$). This is quite similar to rates estimated at lower redshifts within the very large uncertainty (e.g., Barger, Cowie, & Richards 2000, and references therein).

Perhaps of most interest, given this is a single object and statistical inferences are therefore difficult, is that the presence of even a single object at this redshift may suggest we have not yet reached the redshift of reionization. In a pre-reionization epoch the radiation damping wings from the neutral gas will black out regions extending about 20 Å to the redward of the Ly α wavelength in the observed frame of the object (Miralda-Escudé 1998; Miralda-Escudé & Rees 1998). While ultraluminous quasars can ionize their surroundings and prevent this effect, it is unlikely that a small Ly α emitting galaxy of the present type could do this though it could lie in a large ionized region produced by some other source of ionizing photons.

This work was supported in part by the State of Hawaii and by NSF grant AST-0071208 and NASA grant GO-7266.01-96A from Space Telescope Science Institute, which is operated by AURA, Inc., under NASA contract NAS 5-26555. RGM thanks the Raymond and Beverly Sackler Foundation for support. We thank Amy Barger for taking additional LRIS R -band images of A370 to improve our non-detection limits.

REFERENCES

- Anderson, S. F. et al. 2001, *AJ*, 122, 503, astro-ph/0103228
Barger, A. J., Cowie, L. L., & Richards, E. A. 2000, *AJ*, 119, 2092, astro-ph/0001096
Becker, R. H. et al. 2001, *AJ*, 122, 2850, astro-ph/0108097
Bézecourt, J., Kneib, J.-P., Soucail, G., & Ebbels, T. M. D. 1999, *A&A*, 347, 21, astro-ph/9810199
Casali, M., & Hawarden, T. 1992, *JCMT-UKIRT Newsletter*, 4, 33
Cowie, L. L., & Hu, E. M. 1998, *AJ*, 115, 1319, astro-ph/9801003
Dey, A., Spinrad, H., Stern, D., Graham, J. R., & Chaffee, F. H. 1998, *ApJ*, 498, L93, astro-ph/9803137
Ellis, R., Santos, M. R., Kneib, J., & Kuijken, K. 2001, *ApJ*, 560, L119, astro-ph/0109249
Fan, X. et al. 2000, *AJ*, 120, 1167, astro-ph/0005414
Fan, X. et al. 2001, *AJ*, 122, 2833, astro-ph/0108063
Hu, E. M., Cowie, L. L., & McMahon, R. G. 1998, *ApJ*, 502, L99, astro-ph/9803011
Hu, E. M., McMahon, R. G., & Cowie, L. L. 1999, *ApJ*, 522, L9, astro-ph/9907079
Kennicutt, R. C., Jr. 1983, *ApJ*, 272, 54
Kneib, J.-P., Mellier, Y., Fort, B., & Mathez, G. 1993, *A&A*, 199, 273, 367
Landolt, A. U. 1992, *AJ*, 104, 340
Mellier, Y., Soucail, G., Fort, B., & Mathez, G. 1988, *A&A*, 199, 13
Miralda-Escudé, J. 1998, *ApJ*, 501, 15, astro-ph/9708253
Miralda-Escudé, J., & Rees, M. J. 1998, *ApJ*, 497, 21
Motohara, K. et al. 1998, *Proc. SPIE* 3354, 659
Oke, J. B. 1990, *AJ*, 99, 1621
Oke, J. B. et al. 1995, *PASP*, 107, 375
Songaila, A. & Cowie, L. L. 2002, *AJ*, in press (astro-ph/0202165)
Stern, D., & Spinrad, H. 1999, *PASP*, 111, 1475, astro-ph/9912082
Thommes, E. 1999, in *From Stars to Galaxies to the Universe*, ed. G. Boerner & H. Mo, (Garching: MPIA), 120, astro-ph/9812223
Turnshek, D. A., Bohlin, R. C., Williamson II, R. L., Lupie, O. L., Koornneef, J., & Morgan, D.H. 1990, *AJ*, 99, 1243
van Breugel, W. J. M., de Breuck, C., Stanford, S. A., Stern, D., Röttgering, H., & Miley, G. 1999, *ApJ*, 518, L61, astro-ph/9904272
Weymann, R. J., Stern, D., Bunker, A., Spinrad, H., Chaffee, F. H., Thompson, R. I., & Storrie-Lombardi, L. J. 1998, *ApJ*, 505, L95, astro-ph/9807208